THE EFFECT OF SURFACE FUNCTIONALIZED CARBON NANOTUBES ON THE MORPHOLOGY, AS WELL AS THERMAL, THERMOMECHANICAL, AND CRYSTALLIZATION PROPERTIES OF POLYLACTIDE

James Ramontja[1, 2], Suprakas Sinha Ray[1, 2], Sreejarani K. Pillai[1] and Adriaan S Luyt[2]
[1]DST/CSIR Nanotechnology Innovation Centre, National Centre for Nano-Structured Materials, Council for Scientific and Industrial Research, Pretoria 001, South Africa.
[2]Department of Chemistry, University of the Free State (Qwaqwa Campus), Phuthaditjhaba, South Africa.

ABSTRACT

This paper discusses various properties of Poly(lactide) upon nanocomposite formation with functionalized multiwalled carbon nanotubes (f-MWCNTs). The composite was prepared through melt extrusion technique. Functionalization of carbon nanotubes and possible interaction with PLA chains was investigated through attenuated total reflectance (ATR) Fourier transformed-infrared (FT-IR) and Raman spectroscopies. Scanning electron microscope (SEM) and polarized optical microscope (POM- in melt state) also revealed homogenous dispersion of f-MWCNTs in the PLA matrix with some agglomerates. Melting and crystallization phenomena of the nanocomposite studied through differential scanning calorimeter (DSC), wide angle X-ray scattering (WAXS), and POM show that f-MWCNTs facilitates nucleation and crystal growth of PLA matrix significantly. Thermogravimetric analyses (TGA) reveal that overall thermal stability of PLA matrix improves slightly upon the nanocomposite formation. Thermomechanical analyses also reveal a significant increase in modulus of the nanocomposite at room temperature, which drops suddenly across glass transition temperature. This is an indication of plasticization effect.

INTRODUCTION

Over the last two decades, the world has embarked on a massive research in the field of biodegradable and biocompatible polymers, both for medical and ecological applications.[1] One such polymer is polylactide (PLA), for it is readily biodegradable and is made from agricultural sources[2]. PLA has potential medical applications such as tissue culture, surgical implants, restorable sutures, wound closure, and controlled-release systems.[3-5] Polylactide is not only biocompatible but also bioresorbable. When implanted in living organisms including human body, it is hydrolyzed to its constituent α-hydroxy acid which is eliminated by general metabolic pathways[6]. However, for biomedical applications, neat PLA might not be suitable for high load bearing applications[7], which intrigued the need to incorporate the reinforcements such as oriented PLA fibers. Nanocomposites represent an exceptional case of composites in which interfacial relationship between two phases is maximized.

In recent years, a significant amount of work has been done on the preparation and characterization of polymer nanocomposites based on nanoclays such as montmorillinite, saponite, and synthetic mica.[8-14] These fillers moderately improved the mechanical and physical properties of the neat polymer matrices even though their amounts were small (~5 wt.%). The main reason for these improved properties in the case of the clay-containing polymer nanocomposites is the presence of interfacial interactions as opposed to the conventional composites.

Currently a number of researchers are focusing on the preparation and characterization of functionalized carbon nanotube containing polymer nanocomposites.[15-27] This is because CNTs have superior mechanical properties such as extraordinary high strength, high modulus, excellent electrical conductivity along with their thermal conductivity and stability, and the low density associated with high aspect ratio compared to other nano-fillers.[28,29] However, the effective utilization of CNTs has not being realized due to difficulties in producing CNT/polymer nanocomposites with homogeneously well-dispersed CNTs.[30] Due to intrinsic van der Waals interactions,[31] the as received CNTs tend to aggregate and entangle together spontaneously when blended directly with polymers. With poor dispersion, the active surface area for polymer/CNT surface interaction will not increase sufficiently and as a result very small amount of stress will be transferred between CNT filler and polymer matrix. It has been reported that chemical modification on the surface of CNTs improves their dispersion on polymer matrices.[32-36] This chapter summarizes various properties of a PLA composite containing 0.5 wt.% of f-MWCNTs. The f-MWCNTs used in this work contain ~20% (determined gravimetrically) of hexadecylamine (HDA).

EXPERIMENTAL

Materials

PLA (weight average molecular weight = 188k $g.mol^{-1}$) with a *D*-lactide content of 1.1–1.7% was obtained from Unitika Co. Ltd, Japan. Prior to use, PLA was dried at 80 °C for 2 days under vacuum. The CNTs (here multi-walled CNTs) used in this study were synthesized by chemical vapour deposition (inner diameter ~10 nm; outer diameter ~ 20 nm; average length ~500 μm, measured by transmission electron microscopy) and 95% pure (measured by energy dispersive X-ray spectroscopy). Hexadecylamine (HDA), chloroform, and ethanol were purchased from Sigma-Aldrich and used as received.

In a typical functionalization process, a mixture of 1g CNTs and 5g HDA was taken in a conical flask and heated at 180°C for 6 h in an oil bath. After cooling to room temperature, the excess of HDA was removed from the reaction mixture by washing with ethanol several times. The black solid was then collected by Nylon membrane filtration (0.45 μm pore size) and dried at 110°C overnight to get a constant weight. The increased weight of the CNTs was ~20%, determined gravimetrically. This results imply that the amount of HDA surfactant content is ~20 wt.-%

Preparation of Nanocomposites

For the preparation of PLA/MWCNT nanocomposite, f-MWCNTs (0.5 wt.-%, powder form) and PLA (pellet form) were first dry mixed in a polyethylene bottle. The mixture was then extruded using co-rotating twin-screw mini-extruder (bench-top Haake Minilab II, Thermo Scientific) operated at 180°C (screw speed = 30 rpm, time = 5 min) to yield black nanocomposite strands. These strands were chopped into pieces and stacked between two metal plates and compression molded by pressing with 2 MPa pressure at 180 ^{o}C for 2 min. Neat PLA and nanocomposite samples were annealed at 110 °C under vacuum prior to all characterizations and property measurements.

Characterization and property measurement

The functionalization and the presence of f-MWCNTs was confirmed through the attenuated total reflectance (ATR) Fourier-transform infrared (FT-IR) using Perkin Elmer Spectrum 100 instrument at a resolution of 4.0 cm^{-1}. Raman spectroscopy studies were employed using a lab Raman system, Jobin-Yvon Horiba T64000 Spectroscopy, equipped with an Olympus

BX-40 microscope. The excitation wavelength was 514.5 nm with an energy setting of 1.2 mW from a Coherent Innova model 308 argon ion laser. The morphology of the freeze fractured surface of the composite was analyzed using Carl Zeiss SMT Neon 40, Cross Beam Series FIB-SEM in SEM mode, with an acceleration voltage of 2 kV. The spherulitic growth behaviour and the degree of dispersing in molten state of neat PLA and its composite were studied with a Carl Zeiss Imager Z1M polarized optical microscope (POM). Samples were heated to 190°C at a heating rate of 20°C.min^{-1}, held at that temperature for 5 min, and then the pictures were taken.

The melting and glass transition temperatures as well as crystallinity of the PLA matrix before and after nanocomposite formation were studied with a DSC instrument (model: TA Q2000) under constant nitrogen flow of 50 mL.min^{-1} and a heating rate of 20 ^{o}C.min^{-1}. WAXS experiments of the PLA and nanocomposite samples were carried out in an Anton Paar SAXS instrument operated at 40 kV and 50 mA with line collimation geometry. The radiation used was a Ni filtered CuK_{α} radiation of wavelength 0.154 nm (PAN Analytical X-ray source). Thermogravimetric analyses of both PLA and the nanocomposite samples were carried out on a TGA Q500 (TA Instruments) at a heating rate of 10 ºC.min^{-1} under thermo-oxidative conditions, from ambient temperature to 650 ºC. The dynamic mechanical properties of neat PLA and its composite samples were determined using an Anton Paar-Physica MCR501 Rheometer in the tension-torsion mode. The temperature dependence of the storage modulus (G´) and tan δ of neat PLA and composite samples, were measured at a constant frequency (ν) of 6.28 rad.s^{-1} with the strain amplitude of 0.02% (selected after a series of strain sweep tests at different temperatures to determine the linear region) and in the temperature range of -20 to 160 ºC at a heating rate of 2 ºC.min^{-1}.

RESULTS AND DISCUSSION

Attenuated total reflectance fourier-transform infrared (ATR-FTIR) spectroscopy

Figure 1 shows the ATR-FTIR spectra of neat PLA, the f-MWCNTs and the PLA/f-MWCNTs composite. The spectrum of the composite shows the characteristic peaks of PLA and the f-MWCNTs. The broad peak in the spectrum of the f-MWCNTs represents the N-H stretching of HDA. This broad peak also appears in the spectrum of the composite. The peak at 1592 cm^{-1} (indicated by *) in the spectrum of the f-MWCNTs represents the primary amine N-H deformation of HDA. This peak is also observed in the spectrum of the composite at 1645 cm^{-1} (also indicated by *). These results confirm the presence of f-MWCNTs in the composite. However, it is difficult to establish whether there is a possible interfacial interaction between the PLA and the HDA chains, because we could not get a clear peak of the N-H stretching in both the f-MWCNTs and the composite spectra.

Raman spectroscopy

Raman spectroscopy was used to verify the presence of possible interfacial interactions between f-MWCNTs and the matrix of PLA. Figure 2 shows the Raman spectra of the f-MWCNTs and the corresponding nanocomposite of PLA. It can be seen from the spectra that there is a small shift in the characteristic *D*-band and a quite significant shift in the *G*-band of the f-MWCNTs to higher wavenumbers in the case of the nanocomposite. This indicates the presence of interfacial interactions between the PLA chains and the f-MWCNTs surfaces. It can also be seen that the characteristic peak of the PLA matrix (appearing at 1450 cm^{-1} for neat PLA,

[26]) moves toward higher a wavenumber of 1453 cm^{-1}. This observation further confirms the presence of some interactions between the PLA matrix and the f-MWCNT surfaces.

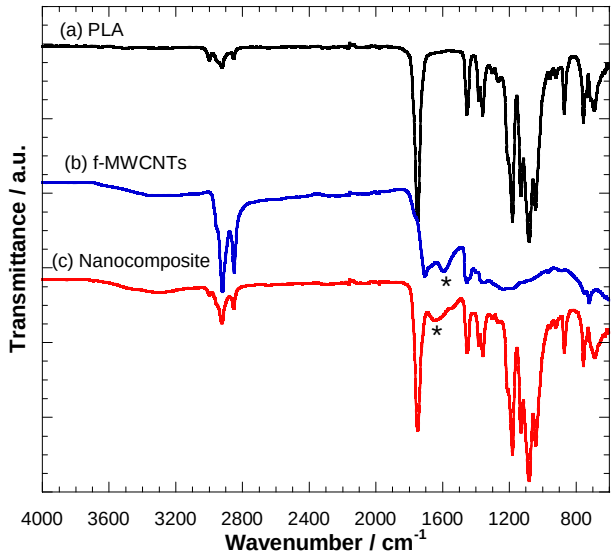

Figure 1. FT-IR spectra of pure PLA, f-MWCNTs, and the nanocomposite.

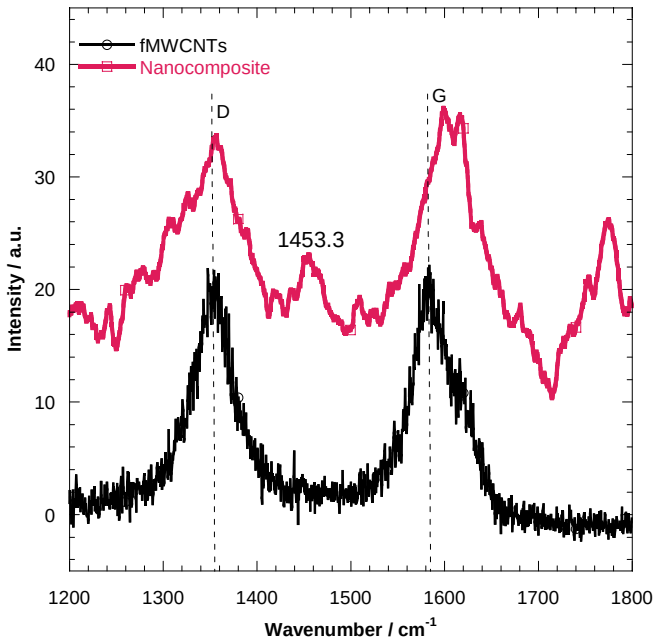

Figure 2. Raman spectra of PLA and its nanocomposite.

Scanning electron microscopy

The dispersion of the f-MWCNTs in the PLA matrix was studied using a scanning electron microscope (SEM) operated at an accelerated voltage of 2 kV. figure 3 (a) represents the SEM image of the freeze fractured surface of the PLA/f-MWCNT nanocomposite. The polymer

matrix surface with some white spots is clearly seen. Two areas, with and without white spots, were selected and magnified. They are shown in figure 3(b & c). In these pictures a fairly good dispersion of CNTs can be seen, but the white spots are clearly the result of agglomeration of f-MWCNTs in the PLA matrix at a micron scale level. Agglomeration of MWCNTs in the PLA matrix suggests that part of the surface area of CNTs could not be accessed during functionalization by HDA. This is due to the intrinsic van der Waals forces keeping the MWCNTs together as bundles. Based on these observations, it can be concluded that the homogenous dispersion of the f-MWCNTs is the result of improved interaction between the PLA matrix and the HDA chains on the surface of the MWCNTs, as established in Raman results.

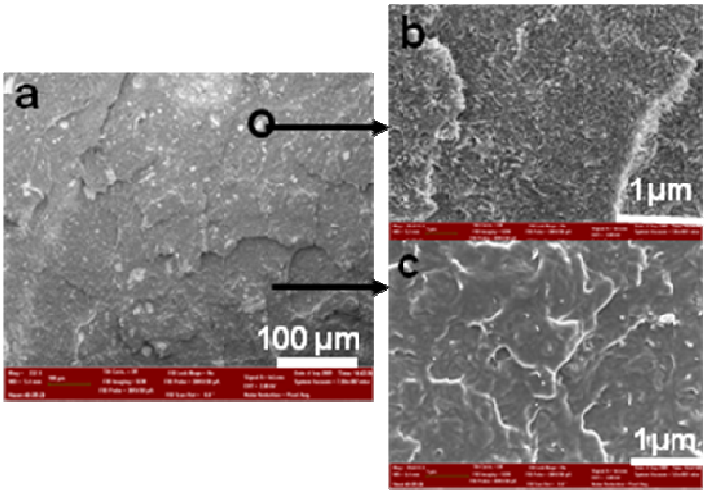

Figure 3.Scanning electron microscopy images of a nanocomposite containing 0.5 wt.% f-MWCNTs with two selected spots at different magnifications.

Polarized optical microscopy

To further verify the good dispersion of the f-MWCNTs in the PLA matrix, the composite was investigated through an optical microscopy at 190 ºC where PLA was in the molten state. These results are presented in figure 4. The dark spots represent agglomerates of CNTs. This image clearly shows that there is an improved dispersion of f-MWCNTs with few agglomerates at micron scale, as shown by the dark spots. Again, this results support the SEM results.

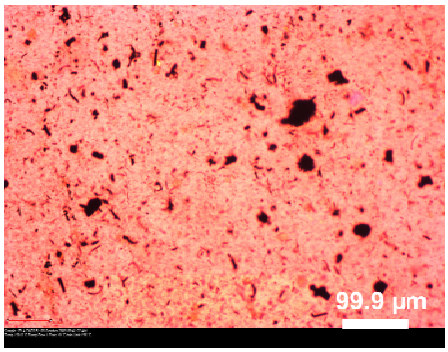

Figure 4. Optical microscopic image of the PLA/f-MWCNTs nanocomposite taken at 190 ºC in the transmittance mode. This is the representative image of images taken from five different positions.

The effect of cooling rate on the non-isothermal crystallization behaviour of PLA

To study the influence of cooling rates on the non-isothermal crystallization behaviour of PLA, the samples were heated to 190 °C at a heating rate of 20 °C.min^{-1}, kept at this temperature for 5 min, and then cooled down to -20 ºC at different cooling rates. The cooling curves of pure PLA and its composite during non-isothermal crystallization from their melts at five different cooling rates are shown in figure 5. In the case of neat PLA, a broad peak is observed when the sample was cooled from the melt at a rate of 0.5 ºC.min^{-1}. With an increase in cooling rate to 1 °C.min^{-1}, a peak with a shoulder peak appears and shifts towards lower temperatures. The peak shoulders indicate a continuous change of enthalpy. It is clear that at cooling rates higher than 5 ºC.min^{-1}, it is very difficult for the PLA matrix to fully crystallize and the polymer stays in a super-cooled state. The crystallization peak shifts to lower temperatures as the cooling rate is increased is a natural observation, because it is difficult for the polymer chains to crystallize at faster cooling rates. A small crystallization peak appears at 126 ºC for the composite when the cooling rate from the melt is 0.5 ºC.min^{-1}. It is further observed that this peak does not clearly show the double thermal event that was observed in the case of the neat PLA. This peak also shifts to lower temperatures as the cooling rate increases to 1 ºC.min^{-1}. A further increase in the cooling rates to 5 ºC.min^{-1} also shows the presence of a double peak as in the case of PLA. The crystallization peaks for the nanocomposite, for all the investigated cooling rates, are more intense and better resolved than those for neat PLA. What is more interesting is that even at a faster cooling rate of 10 ºC.min^{-1}, the nanocomposite is still able to crystallize. Based on the observations above, it can be concluded that f-MWCNTs act as nucleating agents for the crystallization of the PLA matrix.

To confirm the nucleating effect of the f-MWCNTs during non-isothermal crystallization, the samples were investigated through POM. For the POM measurements, a cooling rate of 10 ºC.min^{-1} was selected because during injection moulding the cooling rates are usually very fast. The POM images of the PLA and its nanocomposite, taken at 130 ºC during isothermal crystallization from their melt, are shown in figure 6. The images show large spherulites for the neat PLA sample, but much smaller and more densely packed crystallites for the nanocomposite. This observation indicates that the f-MWCNT nanoparticles formed nucleating sites for the formation of small spherulites in the nanocomposite.

Effect of cooling rates on melting behaviour of PLA

In order to study the effect of cooling rates on the melting behaviour, PLA and its nanocomposite were heated from -20 to 190 °C at 20 °C.min^{-1} as soon as the cooling was finished. These heating curves are presented in figure 7, and the DSC data are summarized in Table 1. It can be seen that PLA only shows cold crystallization peaks and two melting peaks when the cooling rates were 5 and 10 ºC min^{-1}. The composite also shows cold crystallization peaks at the same cooling rates, but single melting peaks. This observation indicates that the crystallization of PLA chains was not completed during cooling at the faster cooling rates, and the crystallization process continued during heating. The double melting peaks indicate the presence of different types of crystals with different stabilities. Nam *et al.*[27] also suggested that the double melting peaks of PLA may be due to the presence of less perfect crystals having enough time to melt and rearrange into crystals with higher structural perfection, which re-melted at higher temperatures during heating in the DSC. However, when the cooling rates were 0.5, 1, and 2 ºC.min^{-1}, no cold crystallization peak was observed for both PLA and its nanocomposite. This indicates that the crystallization of PLA chains was completed at slower

cooling rates during the non-isothermal cooling process. Single melting peaks were observed when the cooling rate was 0.5 °C.min^{-1} for both samples. In brief, the nanocomposite shows two distinct melting peaks when the cooling rate was 2 °C.min^{-1} in comparison to the neat polymer. This is an indication that the nucleation effect of f-MWCNTs in the polymer matrix assisted in the formation of more perfect crystals.

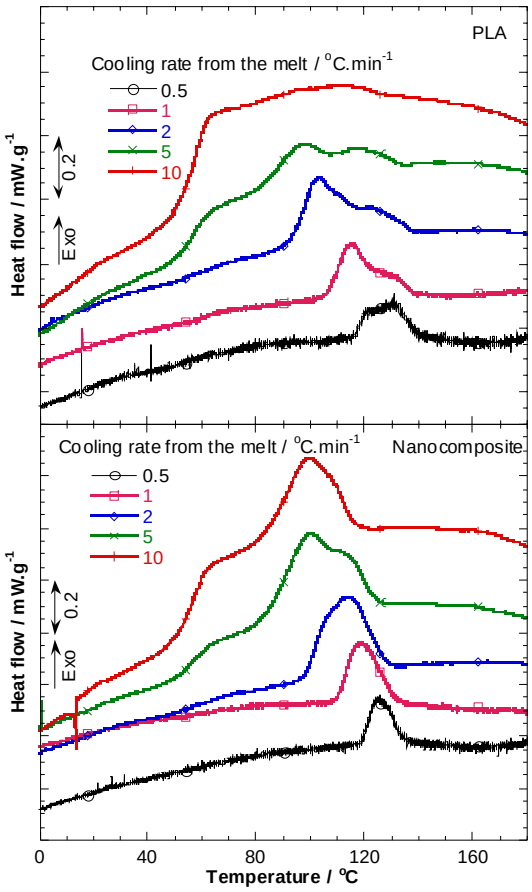

Figure 5. DSC heating curve of PLA and its nanocomposite after non-isothermal crystallization at different cooling rates.

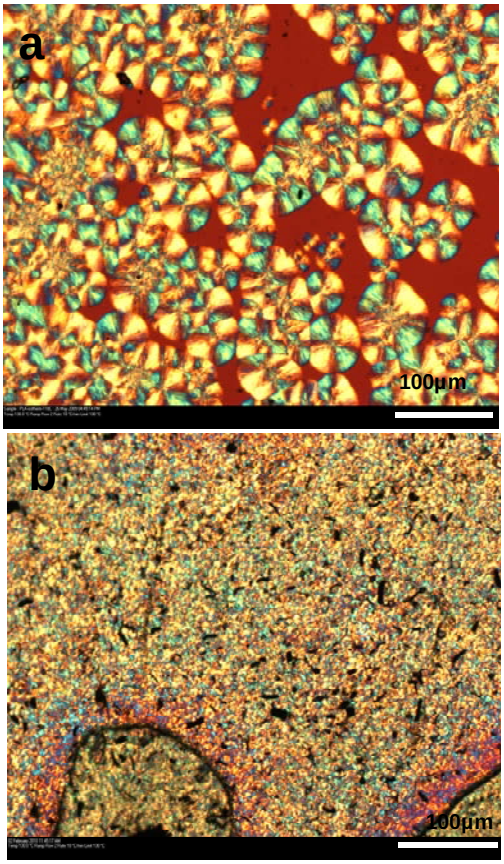

Figure 6. Polarized optical micrographs of (a) neat PLA and (b) the PLA/f-MWCNT nanocomposite. Both samples were crystallized at 130 °C from their melts.

By integrating the area under the endothermic region of the DSC curves, and by subtracting the extra heat absorbed by the crystallites formed during cold crystallization, the melting enthalpy (ΔH_m) of all the samples was calculated, and at the same time the degree of crystallinity (χ_c) was estimated by considering the melting enthalpy of 100% crystalline PLA as 93 J.g^{-1}.[21] The χ_c data in Table 1 show that the overall crystallinity of PLA was reduced when 0.5 wt.% f-MWCNTs was added. A decrease in overall crystallinity may be as a result of two factors: MWCNT agglomerates acting as active nucleation sites and at the same time, the non-agglomerated sites inhibiting mobility of the polymer chains. Because of the well-dispersed f-MWCNTs crystal growth was inhibited, thus leading to a decrease of crystallinity.

Table 1 Cooling rate dependence of the melting enthalpy from two melting peaks of the PLA and the composite

Sample	Cooling rate	Melting enthalpy / J g^{-1} [a]	% crystallinity[b]
PLA	0.5	53.0	57.0
	1	44.4	47.8
	2	41.1	44.2
	5	37.6	40.4
	10	37.6	40.4
Nanocomposite	0.5	48.0	51.6
	1	40.1	43.1
	2	39.1	42.0
	5	38.8	41.7
	10	33.9	36.5

[a] The total melting enthalpy of PLA evaluated by integration of the area under the endothermic peaks from the heating scans after non-isothermal crystallization.
[b] Calculated using the melting enthalpy of 100% crystalline PLA, 93 J g^{-1}.[37]

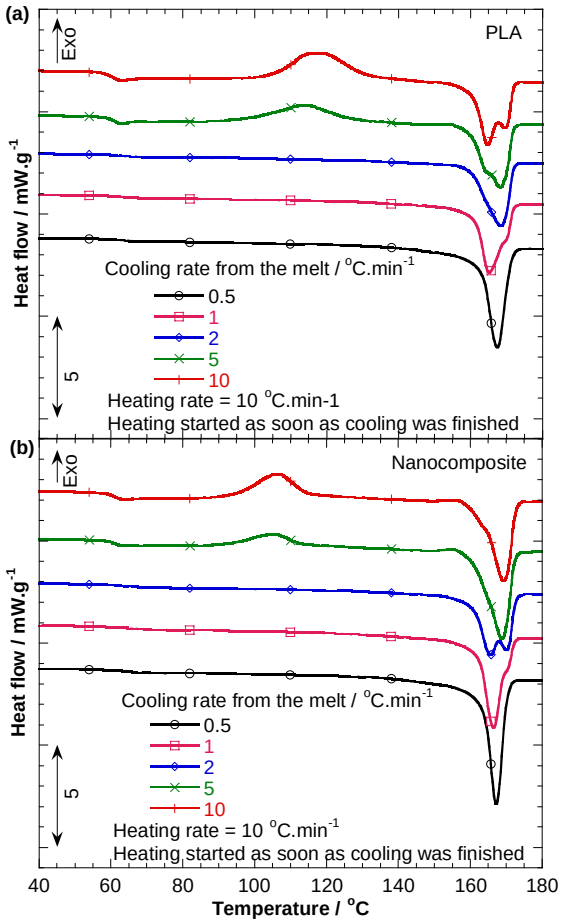

Figure 7. DSC heating curves of PLA and the nanocomposite after non-isothermal crystallization at five different cooling rates.

Temperature modulated DSC

To separate the heat capacity and kinetically related components during cold crystallization and subsequent melting of neat PLA and its nanocomposite, TMDSC of melt quenched samples were done. TMDSC allows us to see whether any re-crystallization process occurs as soon as PLA begins to melt. This has been used to confirm the presence of melting, re-crystallization, and re-melting processes. Figure 8 illustrates the TMDSC curves of (a) neat PLA and (b) its nanocomposite during the second heating. The samples were first equilibrated at -20 ^{o}C for 30 min, and then heated to 190 ºC at a rate of 2 ºC.min^{-1}, kept at that temperature for 5 min. to destroy any previous thermal history, and cooled to -20 ^{o}C at a rate of 2 ºC.min^{-1}. TMDSC was started as soon as the cooling was finished. For both samples the total heat flow (middle curve) is separated into well defined reversible heat flow (bottom curve) and non-reversible heat flow (top curve). For neat PLA, the following behaviour is observed: two melting signals on the reversible heat flow curve are accompanied by the subsequent re-crystallization on the non-reversible heat flow curve, with the total heat flow curve showing only the melting peaks. This observation may be due to the partial melting and perfection of different crystals at temperatures before their final melting. For the nanocomposite, two melting peaks are observed for all the heat flow curves with no apparent re-crystallization. What is more notable is that the two melting peaks of the nanocomposite on the reversible heat flow curve are now distinct in comparison with the peaks for the neat polymer. This indicates the presence of different forms of crystals with different thermal stabilities. Another interesting feature is that TMDSC enabled us to see partial re-crystallization occurring in the neat polymer, which is absent in the composite.

To estimate the percent crystallinity (χ_c) of the samples, we took the enthalpy of melting (ΔH_f) from the reversible heat flow curve, divided this value by the enthalpy of a 100% crystalline polymer (ΔH_f for 100 % crystalline PLA is 93 J.g^{-1} [21]), and multiplied the answer by 100%. The data is reported in table 2. These values indicate that the crystallinity of the PLA matrix decreased in the presence of the f-MWCNTs.

Table 2 TMDSC data for PLA and its nanocomposite.

Sample	Total			Reversible				Non-reversible			χ_c
	T_{m1} ºC	T_{m2} ºC	ΔH_f J.g^{-1}	T_g ºC	T_{m1} ºC	T_{m2} ºC	ΔH_f J.g^{-1}	ΔH_c J.g^{-1}	ΔH_f J.g^{-1}	T_m ºC	%
PLA	169.9	-	43.54	62.2	164.2	169.8	30.1	8.9	26.7	169.9	19.1
Composite	165.3	171.2	44.94	62.0	165.3	171.2	26.9	1.7	24.3	171.0	24.3

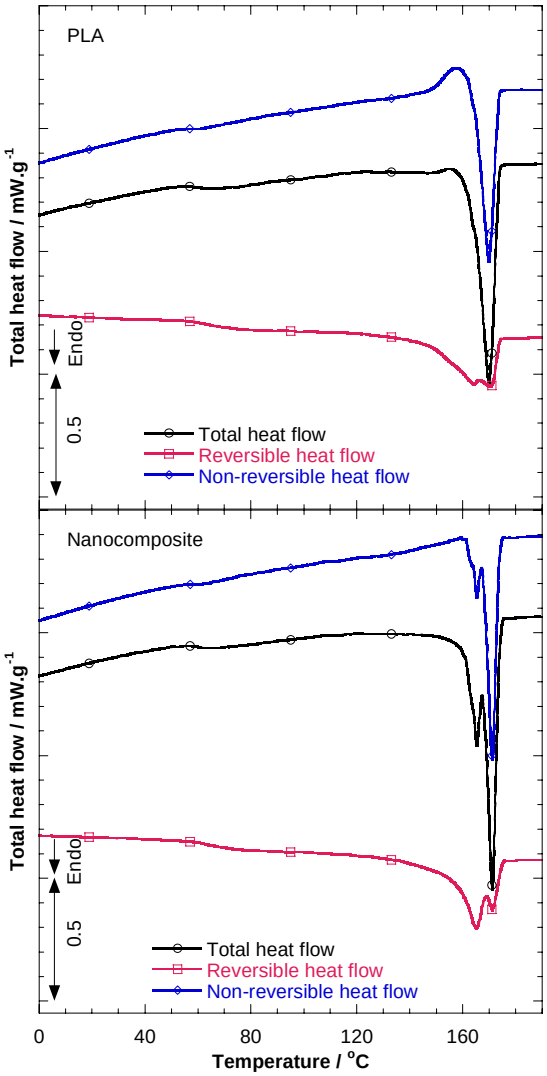

Figure 8. TMDSC curves of (a) PLA and (b) the nanocomposite during second heating.

Wide angle X-ray scattering

To study the presence of different PLA crystals and their modification, WAXS of the neat PLA and nanocomposite samples were performed. The measurements were taken from room temperature to the melting temperature, and then back to room temperature. The samples were kept at each temperature for 5 minutes, including 1 minute exposure to the X-rays. Figure 9 shows the one-dimensional WAXS patterns of PLA and the nanocomposite obtained under these conditions. Overall, there is no sign of the modification of existing crystals or the formation of new crystals. The notable observation is when both samples were cooled from their melts. It is clear that it is very difficult for PLA to crystallize during cooling. However, crystals are formed in the presence of f-MWCNTs as shown by the fully resolved peaks in the spectra of the nanocomposite. Again, this supports the nucleation effect of f-MWCNTs in the polymer matrix. However, a very small peak is observed on the spectra of both samples at around $2\Theta = 22.5^{\circ}$. This observation suggests the growth of another type of crystal.

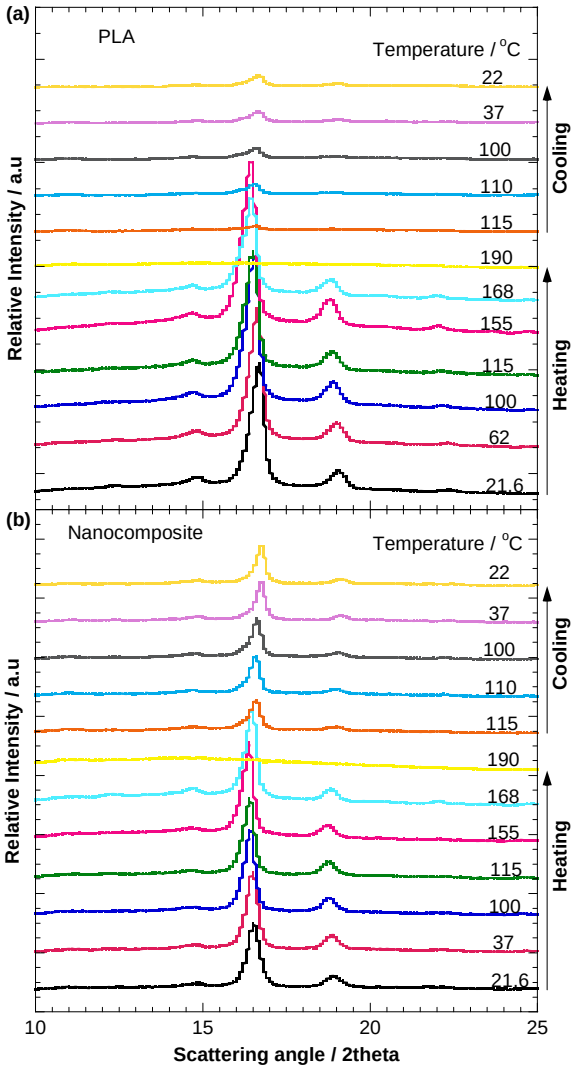

Figure 9. Temperature dependence wide-angle X-ray scattering patterns of (a) neat PLA and (b) the nanocomposite samples during both heating and cooling cycles.

Thermogravimetric analysis

This section discusses the thermal stabilities of neat PLA and the nanocomposite in a thermo-oxidative environment. The TGA and the first dTGA curves of neat PLA and the nanocomposite obtained under oxygen flow are presented in figure 10. The dTGA are presented because they more clearly show the difference in thermal stabilities between the samples. Both samples show a one-step decomposition. The thermal stability of the nanocomposite is higher than that of the neat PLA. This improvement can be attributed to the fairly homogenous dispersion of the f-MWCNTs. The thermal stability of the nanocomposite may also be due to the higher thermal stability of the CNTs in comparison to that of PLA. The dTGA peak of the nanocomposite shifts to a higher temperature compared to that of the neat PLA sample. This is also an indication of the improvement in thermal stability of PLA in the presence of the f-MWCNTs.

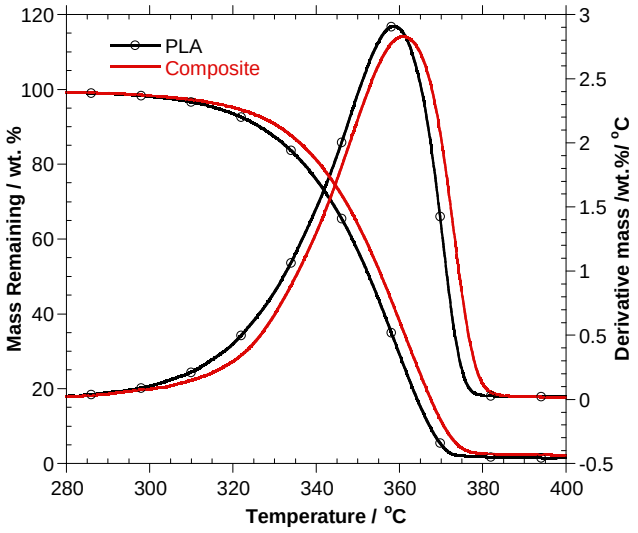

Figure 10. TGA and derivative TGA curves of PLA and the nanocomposite under oxygen flow at a heating rate of 10 ºC min^{-1}.

Dynamic mechanical analysis

DMA generally reveals the amount of energy stored in the nanocomposite as elastic energy, and the amount of energy dissipated during mechanical strain, which strongly depends on the geometrical characteristics and the level of dispersion of the filler in the matrix. It also depends on the degree of interaction between the matrix and the filler.[38] Figure 11 (a and b) represents the storage modulus (G') and the damping factor (tan δ) curves for PLA and the nanocomposite, respectively. The damping factor provides information on the relative contributions of the viscous and elastic components of the viscoelastic material. Figure 11a shows three phenomena: (1) from 0-50 ºC, there is an increase in modulus. This is because both samples are stiff because there is not yet chain mobility, but the nanocomposite is stiffer due to the presence stiff f-MWCNTs; (2) from 50-80 ºC, there is a sudden drop of modulus because the chains of the surfactant (HDA) exhibits a plasticizing effect on the polymer matrix just below and above the glass transition temperature; (3) from 80-160 ºC, there is a slight improvement of modulus because the presence of fairly homogenously dispersed f-MWCNTs inhibits the PLA chain mobility. Figure 11b clearly indicates that there is a decrease in the glass transition temperature from 74 to 71 ºC. This supports the observation of a plasticizing effect of the HDA chains in the PLA matrix. From these observations it may be concluded that the fairly homogenously dispersed f-MWCNTs in the PLA matrix improved the storage modulus below and above the glass transition temperature. Also, the f-MWCNTs acted as a plasticizer of the PLA matrix at around the glass transition temperature.

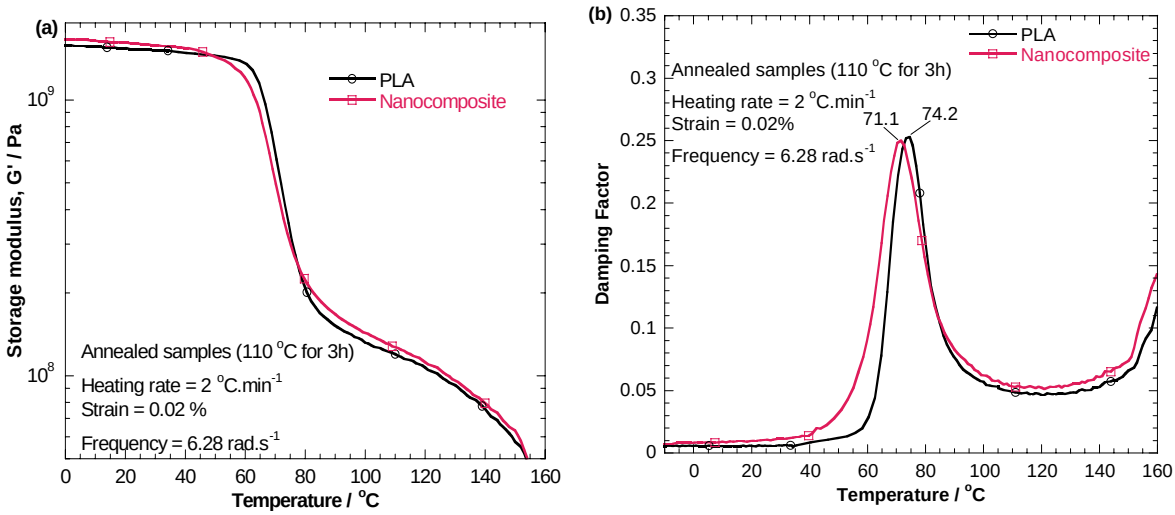

Figure 11. Temperature dependence of dynamic mechanical properties of neat PLA and its nanocomposite: (a) storage modulus and (b) damping factor.

CONCLUSIONS

This paper discussed the morphology, thermal, and thermomechanical properties of a PLA nanocomposite containing 0.5 wt.% of f-MWCNTs (with an amine content of ~20 %). The SEM and POM (of the samples in the molten state) results confirm the homogenous dispersion of f-MWCNTs in the PLA matrix, with some micro-agglomeration. The POM results also show the formation of much smaller PLA crystallites in the presence of f-MWCNTs. The f-MWCNTs were found to play a nucleation role in the crystallization of PLA, as observed from the DSC, SEM, and WAXS results. The DMA and TGA results show that the presence of f-MWCNTs had only a slight influence on the thermomechanical properties and thermal stability of the PLA. FTIR and Raman spectroscopy confirmed the functionalization of the MWCNTs, and the presence of facial interaction between f-MWCNTs and the PLA matrix.

ACKNOWLEDGEMENTS

We wish to thank the CSIR executive and the DST, South Africa, for financial support.

REFERENCES

[1]Y. Ikada and H. Tsuji, Biodegradable polyesters for medical and ecological applications, *Macomol. Rapid Commun*., **21**, 117-32 (2000).
[2]P. Gruber and M. O'Brien, Polyesters III Applications and Commercial Products, Biopolymers edited by Y. Doi and A. Steinbuchel, Wiley-VCH, Weinheim, vol., **4**, 235 (2002).
[3]V. Krikorian and D. J. Pochan, Poly (L-Lactic Acid)/Layered Silicate Nanocomposite: Fabrication, Characterization, and Properties, *Chem. Mater*, **15**, 4317-24 (2003).
[4]R. A. Jain, The manufacturing techniques of various drug loaded biodegradable poly(lactide-*co*-glycolide) (PLGA) devices, *Biomaterials*., **21**, 2475-90 (2000).
[5] K. R. Kamath and K. Park, Biodegradable hydrogels in drug delivery, *Adv. Drug Delivery Rev*., **11**, 59-84 (1993).
[6](a) E. J Frazza, E. E Schmitt, A new absorbable suture, *J. Biomed. Mater. Res. Symp*., **1**, 43-58 (1971). (b) M Vert, Biomedical Polymers from Chiral Lactides and Functional. Lactones: Properties and Applications, *Makromol. Chem., Makromol. Symp*., **6**, 109 (1986).

[7]N. C. Bleach, S. N. Nazhat, K. E. Tanner, M. Kellomaki, and P. Tormala, Effect of filler content on mechanical and dynamic mechanical properties of particulate biphasic calcium phosphate polylactide composites *Biomaterials*., **23**, 1579-85 (2002).
[8]S. Sinha Ray, P. Maiti, M. Okamoto, K. Yamada, and K. Ueda. New polylactide/layered silicate nanocomposites. I. Preparation, characterization and properties. *Macromol*., **35**, 3104–10 (2002).
[9]S. Sinha Ray, K. Yamada, M. Okamoto, A. Ogami, and K. Ueda, New polylactide/layered silicate nanocomposites. 3. High performance biodegradable materials, *Chem. Mater*., **15**, 1456–65 (2003).
[10]S. Sinha Ray, K. Yamada, M. Okamoto, and K. Ueda. Biodegradable polylactide/montmorillonite nanocomposites, *J. Nanosci. Nanotech*., **3**, 503-10 (2003).
[11]C.R. Tseng, J.Y. Wu, Y.H. Lee, and F.C. Chang, Preparation and crystallization behaviour of syndiotactic polystyrene-clay nanocomposites, *Polymer*., **42**, 10063-70 (2001).
[12]R.A. Vaia, H. Ishii, E.P. Giannelis. Synthesis and properties of two-dimensional nanostructures by direct intercalation of polymer melts in layered silicates, *Chem Mater*., **5**, 1694-96 (1993).
[13]M. Okamoto, S. Morita, and T. Kotaka. Dispersed structure and ionic conductivity of smectic clay/polymer nanocomposites, *Polymer*., **42**, 2685-88 (2001).
[14]B. Lepoitevin, N. Pantoustier, M. Alexandre, C. Calberg, R. Jerome, and P. Dubois, Polyester layered silicate nanohybrids by controlled grafting polymerization, *J. Mater Chem*., **12**, 3528-32 (2002).

[15]F.T. Fisher, R.D. Bradshaw, and L.C. Brinson, Effects of nanotube waviness on the modulus of nanotube-reinforced polymers, *Appl Phys Lett*., **80**, 4647-49 (2002).
[16]Z. Yao, N. Braidy, G.A. Botton, and A. Adronov, Polymerization from the surface of single-walled carbon nanotubes − Preparation and characterization of nanocomposites *J. Am. Chem. Soc*., **125**, 16015–24 (2003).
[17]S. Qin, D. Qin, W.T. Ford, D.E. Resasco, and J.E Herrera, Functionalization of single-walled carbon nanotubes with polystyrene via grafting to and grafting from methods. *Macromolecules*., **37**, 752–57 (2004).
[18]J. Chen, R. Ramasubramaniam, C. Xue, and H. Liu, A versatile molecular engineering approach to simultaneously enhanced, multifunctional carbon-nanotube–polymer composites, *Adv. Funct. Mater*., **16**, 114-19 (2006).
[19]P. Calvert. Nanotube composites: A recipe for strength, *Nature*., 399, 210-11 (1999).
[20]H.S. Kim, B.H. Park, J.S. Yoon, and H.J. Jin. Thermal and electrical properties of poly(L-lactide)-graft-multiwalled carbon nanotube composites, *Eur. Polym. J*., **43**, 1729–35 (2007).
[21]Y.T. Shieh and G.L. Liu, Effects of carbon nanotubes on crystallization and melting behaviour of poly(L-lactide) via DSC and TMDSC studies, *J. Polym. Scie. B Polym. Phys*., **45**, 1870–81 (2007).
[22]G.X. Chen, H.S. Kim, B.H. Park, and J.S. Yoon, Synthesis of poly(L-lactide)-functionalized multiwalled carbon nanotubes by ring-opening polymerization. *Macromol. Chem. Phys*., **208**, 389–98 (2007).
[23]H. Tsuji, Y. Kawashima, H. Takikawa, and S. Tanaka, Poly(L-lactide)/nano-structured carbon composites: Conductivity, thermal properties, crystallization, and biodegradation, *Polymer*., **48**, 4213–25 (2007).
[24]G.X. Chen and H. Shimizu, Multiwalled carbon nanotubes grafted with polyhedral

oligomeric silsesquioxane and its dispersion in poly(L-lactide) matrix., *Polymer*., **49**, 943–91 (2008).
[25]D. Wu, L. Wu, M. Zhang, and Y. Zhao, Viscoelasticity and thermal stability of polylactide composites with various functionalized carbon nanotubes, *Polym Degrad. Stab*., **93**, 1577–84 (2008).
[26]J. Ramontja, S. Sinha Ray, S.K. Pillai, and A.S. Luyt, High-performance carbon nanotubes reinforced bioplastic, *Macromol. Mater. Eng*., **294**, 839-46 (2009).
[27]J.Y. Nam, S.S. Ray, and M. Okamoto, Crystallization behaviour and morphology of biodegradable polylactide/layered silicate nanocomposite, *Macromol*., **36**, 7126–31 (2003).
[28]S. Iijima, Helical microtubules of graphitic carbon, *Nature*., **354**, 56–58 (1991).
[29]J Gao, M. E Itkis, A Yu, E Bekyarova, B Zhao, and R Haddon, Continuous Spinning of a Single-Walled Carbon Nanotube−Nylon Composite Fiber, *J. Am. Chem. Soc*., **127**, 3847-54 (2005).
[30]E. T. Michelson, C.B. Hoffman, A. G. Finzler, R. E. Smalley, R. H. Hauge, and J. L. Margrave, Fluorination of Single-Wall Carbon Nanotubes, *Chem. Phys. Lett*., **296**(1-2), 188-94 (1998).
[31]D Qian, E. C Dickey, R Andrews, T Rantell, Load transfer and deformation mechanisms in carbon nanotube-polystyrene composites, *Appl. Phys. Lett*., **76**(20), 2868-70 (2000).
[32]J. P Salvetat, A. J Kulik, J. M Bonard, G. A. D Briggs, T Stockli, K Metenier, et al, Elastic Modulus of Ordered and Disordered Multiwalled Carbon Nanotubes, *Adv. Mater*., **11**, 161-65 (1999).
[33]C Park, Z Ounaies, K. A Watson, R. E Crooks, J Smith, and S. E Lowther, Dispersion of single wall carbon nanotubes by in situ polymerization under sonication, *Chem. Phys. Lett*., **364**, 303-08 (2002).
[34]M. L. Chapelle, C. Stephan, T. P. Nguyen, S. Lefrant, C. Journet, P. Bernier, Raman characterization of single-walled carbon nanotubes and PMMA-nanotubes composites, *Synth. Mater*., **103**, 2510-12 (1999).
[35]K Kim, S. J. Cho, S. T. Kim, I. J. Chin, H. J. Choi, Formation of Two-Dimensional Array of Multiwalled Carbon Nanotubes in Polystyrene/Poly(methyl methacrylate) Thin Film, *Macromolecules*., 38, 10623-26 (2005).
[36]S. Sinha Ray, S. Vaudreil, A. Maazouz, and M. Bousmina, Dispersion of multi-walled carbon nanotubes in biodegradable poly(butylene succinate) matrix, *J. Nanosci. Nanotechnol*., **6**, 2191–95 (2006).
[37]E.W. Fisher, H.J. Sterzel, and G. Wegner, Investigation of the structure of solution grown crystals of lactide copolymers by means of chemical reactions. *Kolloid Z.Z. Polym*., **25**, 980-90 (1973).
[38]E.T. Michelson, C.B. Hoffman, A.G. Finzler, R.E. Smalley, R.H. Hauge, and J.L. Margrave, Fluorination of single-wall carbon nanotubes, *Chem. Phys. Lett*., **296**, 188-94 (1998).